

Cite this: *Biomater. Sci.*, 2020, **8**, 6903

## Amyloid-like protein aggregates combining antifouling with antibacterial activity†

Juanhua Tian,<sup>a</sup> Yongchun Liu,<sup>b</sup> Shuting Miao,<sup>b</sup> Qingmin Yang,<sup>c</sup> Xinyi Hu,<sup>b</sup> Qian Han,<sup>b</sup> Li Xue\*<sup>a</sup> and Peng Yang \*<sup>b,d</sup>

Infections related to implanted medical devices have placed a heavy burden on public health and require feasible solutions. In this study, a simple approach is reported to fabricate an antifouling and antibacterial dual-functional coating. One-step aqueous supramolecular assembly of bovine serum albumin (BSA) is employed to immobilize  $\epsilon$ -polylysine ( $\epsilon$ -PL) and form a coating (PTB@ $\epsilon$ -PL). Based on amyloid-like protein aggregation through the rapid reduction of the intramolecular disulfide bonds of BSA by tris(2-carboxyethyl) phosphine, a dense PTB@ $\epsilon$ -PL nanofilm with controllable thickness and  $\epsilon$ -PL loading density can be covered on virtually arbitrary material surfaces by simple aqueous dipping. *In vitro* and *in vivo* experiments show that this coating not only exhibits effective antibacterial activity against Gram-positive/Gram-negative bacteria, but also imparts excellent antifouling property to the surface. As a pure biopolymer coating, the PTB@ $\epsilon$ -PL nanofilm shows negligible cytotoxicity and hemolysis. In addition, due to the various functional groups exposed on the surface of the nanofilm, the coating shows excellent interfacial bonding stability and can maintain bactericidal and antifouling properties under harsh conditions including ultrasound, autoclaving, organic solvents, and physiological body fluids.

Received 9th May 2020,  
Accepted 4th July 2020

DOI: 10.1039/d0bm00760a

rsc.li/biomaterials-science

## 1. Introduction

In recent years, impressive advances have been made in implantable biomedical devices that can perform healthcare monitoring, local drug release,<sup>1–4</sup> and assisted organ functions.<sup>5,6</sup> At the same time, the issue posed by biomedical-associated infection is considerable, because it causes implant replacement, inflammation of surrounding tissues and even sepsis, placing a heavy medical burden on patients and society.<sup>7</sup> After the bacteria initially adhere to the surface of the substrate, the secreted extracellular matrix gradually encapsulates the bacteria to form a biofilm, which protects the bacteria from antibiotics, disinfectants, and dynamic environments, leading to persistent infection.<sup>8</sup> Traditional antimicrobial surfaces include surfaces that actively attack bacteria, which are modified with metal/metal oxides,<sup>9–11</sup> antibiotics,<sup>12–14</sup> qua-

ternary ammonium compounds<sup>15–18</sup> and other active bactericidal ingredients,<sup>19–21</sup> as well as surfaces that use antifouling materials to prevent the initial adhesion of bacteria.<sup>22,23</sup> However, due to their respective inherent limitations, these surfaces are not very suitable for practical applications. When the active bactericidal surface accumulates bacterial debris and intracellular components, it will not only shield the active functional group but also provide binding sites and nutrients for subsequent bacterial adhesion. For an anti-fouling surface without bactericidal capability, the surface will eventually be contaminated by the biofilm in long-term application.

To solve the above problems, surface polymerization, layer-by-layer assembly (LBL) and mussel-inspired chemistry were used to combine anti-fouling and bactericidal properties into one surface.<sup>24–33</sup> Hierarchical polymer brushes could be constructed by free radical polymerization or photografting to introduce both a bottom bactericidal layer and a top antifouling layer responding to bacteria-induced acidic environments.<sup>24,25</sup> LBL technology involves electrostatic attraction, hydrogen bonding, coordination and other intermolecular interactions to form coatings on the substrate *via* alternative molecular deposition, and then pre-synthesized bactericidal/antifouling agents (*e.g.*, hetero-bifunctional polyethylene glycol ending with carboxyl group and antimicrobial peptide) could be integrated into the LBL coating.<sup>28,29</sup> In addition, polydopamine-based surface modification has been widely used to decorate pre-functionalized polymers and

<sup>a</sup>Department of Urology, The Second Affiliated Hospital of Xi'an Jiaotong University, West Five Road, No. 157, Xi'an 710004, China. E-mail: xueli1979@xjtu.edu.cn

<sup>b</sup>Key Laboratory of Applied Surface and Colloid Chemistry, Ministry of Education, School of Chemistry and Chemical Engineering, Shaanxi Normal University, Xi'an 710119, China. E-mail: yangpeng@snnu.edu.cn

<sup>c</sup>School of Chemistry and Chemical Engineering, Northwestern Polytechnical University, Xi'an 710072, China

<sup>d</sup>State Key Laboratory of Molecular Engineering of Polymers, Fudan University, Shanghai 200438, China

† Electronic supplementary information (ESI) available. See DOI: 10.1039/d0bm00760a

initiators for the next reaction.<sup>30–33</sup> Unfortunately, the construction of the above coatings often involves complex molecular design to introduce specific interfacial adhesion moieties for physical coating or covalently grafting. These complicated and time-consuming procedures may make them unsuitable for scale-up industrial applications. Secondly, the emergence of antibiotic resistance caused by antibiotics and the potential biohazardous catalyst required for the reaction have a negative impact on the biocompatibility of the coating. Moreover, some surfaces can only be used in narrow application conditions. For example, hierarchical polymer brushes that respond to acidic environments are not suitable for intravascular infections and urinary system infections caused by urease-producing bacteria. In this context, the development of new materials with broad-spectrum bactericidal and anti-biofilm properties in a simple way is the challenge to promote practical implications.

Recently, our work revealed that bovine serum albumin (BSA) could undergo a amyloid-like aggregation through reduction of its disulfide bond triggered by tris(2-carboxyethyl) phosphine (TCEP).<sup>34</sup> As a result, the phase-transited BSA (PTB) oligomers aggregate at the solid/liquid and gas/liquid interfaces to form a macroscopic two-dimensional film, which has excellent antifouling property against proteins, carbohydrates, lipids and microorganisms to effectively prevent biofilm formation.<sup>35</sup> Herein, we adopt this facile method to immobilize  $\epsilon$ -polylysine ( $\epsilon$ -PL) on the surface of medical materials so as to integrate both antifouling and antimicrobial capability on a surface.  $\epsilon$ -PL, a typical antimicrobial peptide composed of 25–35 lysine residues, has been approved by the Food and Drug Administration (FDA) as a food preservative in 2003. As a neutral cationic polypeptide,  $\epsilon$ -PL exerts its bactericidal effect through electrostatic adsorption on the bacterial membrane, followed by leakage of the cytoplasm.<sup>36,37</sup> In the present work, it is demonstrated that the resulting PTB@ $\epsilon$ -PL coating takes advantage of both  $\epsilon$ -PL and the PTB nanofilm, typically including the broad-spectrum bactericidal activity of  $\epsilon$ -PL as well as robust interfacial adhesion and anti-fouling function provided by PTB coating. These outstanding advantages allow PTB@ $\epsilon$ -PL to be utilized as a promising multifunctional coating in terms of preventing biomedical-associated infection and extending the service life of various biomedical implants.

## 2. Results and discussion

The fabrication process of the PTB@ $\epsilon$ -PL coating is shown in Fig. 1a. Typically, the phase transition solution of PTB@ $\epsilon$ -PL was freshly prepared by mixing BSA solution (10 mg mL<sup>-1</sup>), TCEP (50 mM at pH 4.5, pH adjusted by 5 M NaOH), and  $\epsilon$ -PL solution (0.1–0.5 g mL<sup>-1</sup>) at the volume ratio of 1 : 1 : 1. By typically incubating the phase transition solution on a material surface for 2 h at 30 °C, the PTB oligomer nanoparticles could be assembled directly on the solid/liquid interface to form the PTB@ $\epsilon$ -PL coating. This strategy is particularly suitable for devices with complicated shapes, *e.g.*, the formation of the

coating on the inner and outer walls of the lumen of a medical tube in one step to prevent the infection caused by intraluminal and extraluminal routes. Studies have shown that the BSA chain has locally positive or negatively charged microregions that could form intermolecular associations with oppositely charged polysaccharides or amino acids.<sup>38,39</sup> In addition, the native form of BSA is negatively charged in a solution below its isoelectric point (pI, 4.7), which also contributes to the interaction between BSA and positively charged  $\epsilon$ -PL. This intermolecular force driven by electrostatic interaction enables  $\epsilon$ -PL to be encapsulated in the nanofilm formed by BSA phase transition. Matrix-assisted laser desorption ionization time-of-flight (MALDI-TOF) spectra showed that the PTB@ $\epsilon$ -PL nanofilm consisted of both  $\epsilon$ -PL with a molecular mass distribution of 3222–4890 Da and BSA with a molecular mass of 66.8 kDa, reflecting the successful immobilization of  $\epsilon$ -PL *via* the BSA phase transition method (Fig. 1b). A method to directly visualize such immobilization could be implemented by adding fluorescein isothiocyanate (FITC)-labeled  $\epsilon$ -PL (FITC- $\epsilon$ -PL) to the phase transition solution. As reflected by fluorescence microscopy, in contrast to weak fluorescence from the simple adsorption of  $\epsilon$ -PL on the surface of bare glass or PTB nanofilm-coated glass samples, the fluorescence from the PTB@ $\epsilon$ -PL nanofilm was obvious, indicating not a simple surface adsorption but a primary immobilization of  $\epsilon$ -PL in the PTB during the formation of the PTB@ $\epsilon$ -PL nanofilm (Fig. S1†).

The far-UV circular dichroism (CD) spectra of the PTB@ $\epsilon$ -PL nanofilm indicated that after the phase transition, the  $\alpha$ -helix peaks of the native BSA at 208 and 222 nm shifted to the peak of the  $\beta$ -sheet structure at 216 nm, while  $\epsilon$ -PL presented an electrostatically expanded conformation<sup>40</sup> (Fig. 1c). The characterization of the Fourier transform infrared (FTIR) spectra in the amide I band of the PTB@ $\epsilon$ -PL nanofilm reflected the deconvoluted peaks at 1618, 1638 and 1690 cm<sup>-1</sup> assigned to  $\beta$ -sheet aggregates,<sup>41,42</sup> which was in contrast to the predominant contribution of  $\alpha$ -helix at 1657 cm<sup>-1</sup>,  $\beta$ -turn at 1671 cm<sup>-1</sup> and 1684 cm<sup>-1</sup> for the mixture of native BSA and  $\epsilon$ -PL<sup>43</sup> (Fig. 1d and Fig. S2†). The CD and FTIR results reflected the loss of the  $\alpha$ -helix secondary structure and the increase of  $\beta$ -sheets during the phase transition, which was similar to that of the pure PTB system without the addition of  $\epsilon$ -PL. We further used Thioflavin T (ThT) staining to monitor the phase transition process, since ThT would exhibit fluorescence enhancement at 484 nm upon binding with  $\beta$ -sheets.<sup>44</sup> The fluorescence intensity of the phase transition solution with the addition of ThT was continuously enhanced until it reached a plateau after 120 min, so the reaction time at 2 h was used for a single-time coating (Fig. 1e and Fig. S3†).

As reported earlier by our group, amyloid-like structures in the phase transition system can strongly adhere to various surfaces, such as metals, polymers and inorganic materials.<sup>41,45</sup> The water contact angle (WCA) and X-ray photoelectron spectra (XPS) of the resultant PTB@ $\epsilon$ -PL coating on glass, silicon wafer (Si), aluminum oxide (Al<sub>2</sub>O<sub>3</sub>), titanium (Ti), silicone rubber and polyetheretherketone (PEEK) showed a consistent WCA of approximately 80° (Fig. 1f and Fig. S4†) and carbon : nitrogen

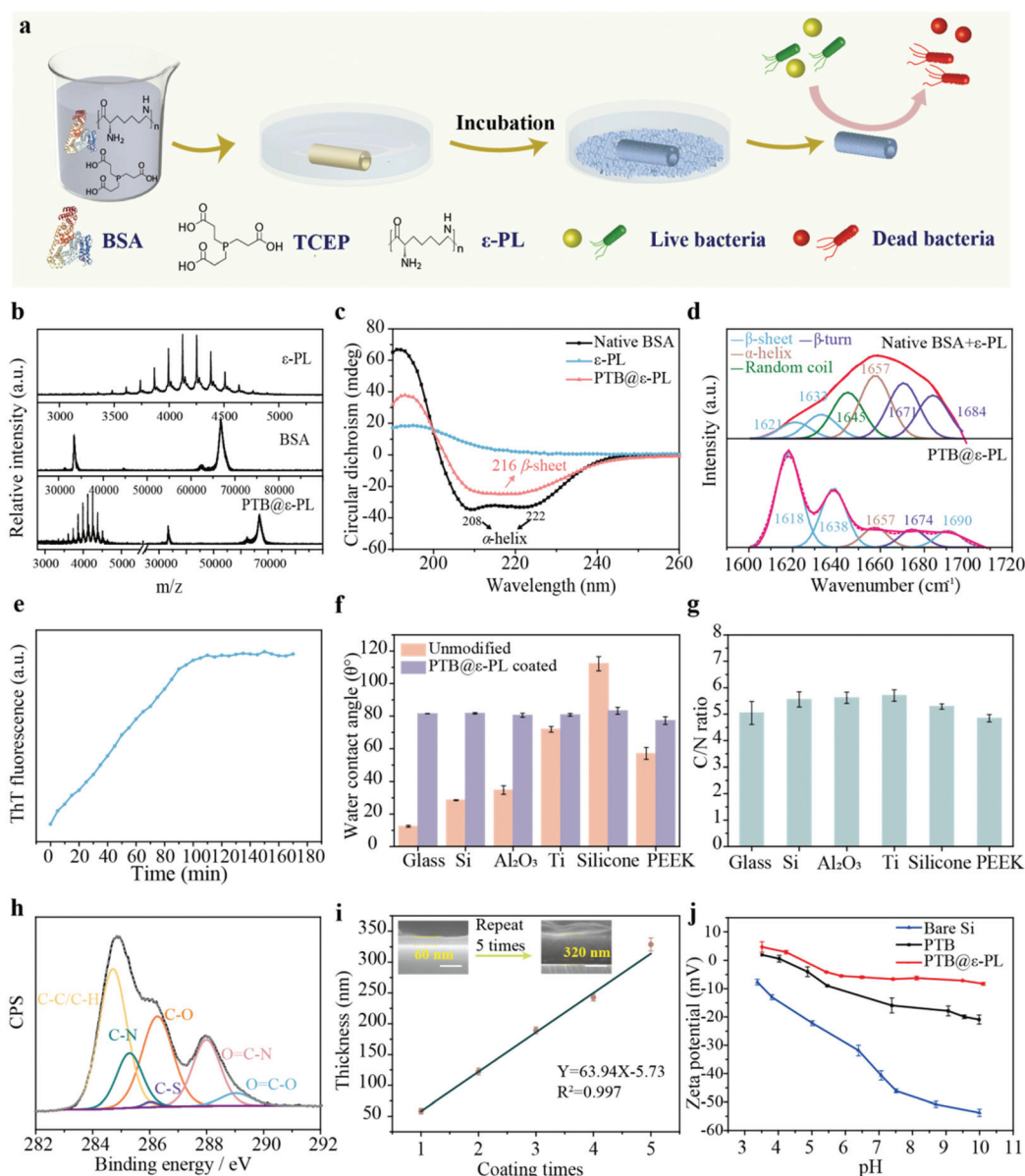


**Fig. 1** The formation of the PTB@ $\epsilon$ -PL coating on various medical substrates. (a) Schematic showing the basic preparation process of the PTB@ $\epsilon$ -PL coating. (b) Typical MALDI-TOF-MS spectra of BSA and  $\epsilon$ -PL in the native state and after the reduction of the BSA disulfide bond by TCEP. (c) CD spectra of native BSA,  $\epsilon$ -PL and the PTB@ $\epsilon$ -PL. (d) FTIR characterization of the mixture of native BSA and  $\epsilon$ -PL, and the PTB@ $\epsilon$ -PL. (e) The fluorescence intensity of the PTB@ $\epsilon$ -PL evolving with the phase transition time by staining the sample with ThT. (f, g) WCA (f) and C : N ratio (g) of the PTB@ $\epsilon$ -PL coating (measured by XPS) on a variety of substrates. (h) High-resolution C 1s XPS spectra of the PTB@ $\epsilon$ -PL nanofilm. (i) The thickness of the PTB@ $\epsilon$ -PL coating varying with the number of repeated coating times. The dip coating method is used to prepare the PTB@ $\epsilon$ -PL coating, and the reaction time for a single coating is 2 h. (j) Zeta potential of PTB@ $\epsilon$ -PL or PTB coating on Si.

(C/N) atomic ratio (Fig. 1g and Fig. S5<sup>†</sup>), indicating that a uniform coating of PTB@ $\epsilon$ -PL formed on these materials (including inert medical materials), which is also confirmed by the Congo red dyeing of the PTB@ $\epsilon$ -PL coating on various materials (Fig. S6<sup>†</sup>). The high-resolution XPS spectra of C 1s reflected the amyloid-like structure inside the PTB@ $\epsilon$ -PL coating favoring the exposure of abundant functional groups on the surface of the nanofilm, mainly including aliphatic carbon (C-C/C-H), amines (C-N), hydroxyl (C-O), amides (O=C-N), thiols (C-S) and carboxyl (O=C-O) groups (Fig. 1h),

which provide robust and universal binding sites with various substrates through coordination, electrostatic, hydrogen bonding and hydrophobic interactions.<sup>39,43</sup> The thickness of the resulting single-time coating is about 60 nm, and as the number of repeated coating times increased, the thickness enlarged almost linearly to hundreds of nanometers (Fig. 1i and Fig. S7<sup>†</sup>). Moreover, single-time PTB@ $\epsilon$ -PL coating and multilayer coatings exhibit a similar surface chemical structure, as reflected by XPS and attenuated total reflection Fourier transformed infrared spectroscopy (ATR-FTIR) (Fig. S8 and

S9†). The zeta potential of the surface indicated that the PTB coating exhibited a weak negative charge at a pH of more than 4.7, which is consistent with the previous study.<sup>35</sup> Due to the introduction of  $\epsilon$ -PL in the nanofilm (the isoelectric point of  $\epsilon$ -PL is about 8.96<sup>40</sup>), the surface charge of the PTB@ $\epsilon$ -PL coating in a wide pH range was closer to neutral than that of the PTB coating, which provided the basis for its antifouling property.<sup>46</sup>

To further investigate the bactericidal performance of the PTB@ $\epsilon$ -PL coating, we adjusted the number of coating times, the initial feeding concentration of BSA and  $\epsilon$ -PL in the phase transition solution, and also replaced  $\epsilon$ -PL with FITC- $\epsilon$ -PL in the phase transition solution to evaluate the average loading density of  $\epsilon$ -PL in the nanofilm by fluorescence spectra quantification. As shown in Fig. 2a and Fig. S10,† by increasing the repetitive coating times, the density of  $\epsilon$ -PL immobilized by the coating and the cumulative release at the same time point were also increased, so the bactericidal activity of the PTB@ $\epsilon$ -PL coating against *Staphylococcus aureus* (*S. aureus*) was enhanced. When the substrate was dip-coated with PTB@ $\epsilon$ -PL 5 times, 96.11% of *S. aureus* could be killed. As proved by our previous work,<sup>41,47</sup> the densely packed oligomer particles in the PTB would make the coating have a tortuous nanochannel structure, so the encapsulated  $\epsilon$ -PL could be gradually released to kill bacteria. It is further deduced that the increase of the  $\epsilon$ -

PL concentration in the phase transition solution would have a positive effect on the bactericidal activity. For a given 5-layer PTB@ $\epsilon$ -PL coating and BSA with an initial concentration of 10 mg mL<sup>-1</sup> in the phase transition solution, the bactericidal ratio against *S. aureus* increased from 54.3 ± 6.8% to 96.5 ± 1.1% with the concentration of  $\epsilon$ -PL changing from 0.1 to 0.4 g mL<sup>-1</sup>, while the bactericidal activity of PTB coating without  $\epsilon$ -PL was negligible. Correspondingly, as the  $\epsilon$ -PL feeding concentration increased from 0.1 to 0.4 g mL<sup>-1</sup>, the average loading density of  $\epsilon$ -PL in the PTB@ $\epsilon$ -PL nanofilm varied from 11.67 to 26.79  $\mu$ g cm<sup>-2</sup>, representing 16.73 nm<sup>-2</sup> to 38.39 nm<sup>-2</sup> in the coating (Fig. 2b and Fig. S11 and S12†). However, when the  $\epsilon$ -PL concentration is more than 0.4 g mL<sup>-1</sup>, the resultant increase on the average loading density of  $\epsilon$ -PL was no longer obvious. Keeping the concentration of  $\epsilon$ -PL at 0.4 g mL<sup>-1</sup>, when the concentration of BSA in the phase transition solution increased from 5 to 20 mg mL<sup>-1</sup>, the most effective bactericidal ratio and the maximum  $\epsilon$ -PL density per unit area were observed in the group with a BSA concentration of 10 mg mL<sup>-1</sup> (Fig. 2c and Fig. S12†). Moreover, we also observed that with the increase of BSA concentration, the surface of the PTB@ $\epsilon$ -PL nanofilm became rougher (Fig. S13†), and the excessively rough surface had a negative effect on the resistance to bacterial adhesion.<sup>48</sup> In addition to *S. aureus* and *E. coli*, *Proteus mirabilis* (*P. mirabilis*) was also used to detect

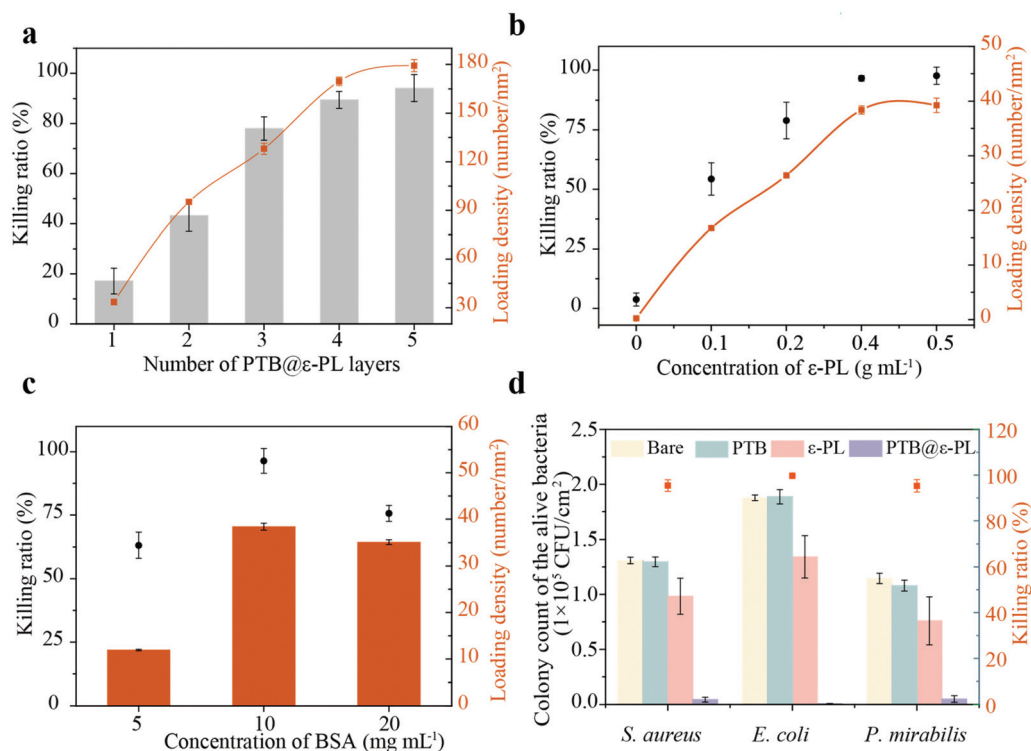


**Fig. 2** *In vitro* bactericidal activity of the PTB@ $\epsilon$ -PL coating. (a) Effect of the repetitive coating times on the bactericidal effect against *S. aureus* and the average loading density of  $\epsilon$ -PL immobilized in the PTB@ $\epsilon$ -PL nanofilm. (b, c) The average loading density of  $\epsilon$ -PL immobilized in the PTB@ $\epsilon$ -PL nanofilm and the corresponding killing efficiency against *S. aureus* at different initial feeding concentrations of  $\epsilon$ -PL (b) and BSA (c). (d) Bactericidal effect of the PTB,  $\epsilon$ -PL adsorption layer on glass and PTB@ $\epsilon$ -PL coating against *S. aureus*, *E. coli* and *P. mirabilis* (bare glass was used as the control group). The data are shown as mean  $\pm$  SD.  $n = 5$  per group.

the bactericidal effect of the PTB@ $\epsilon$ -PL coating *in vitro*, given that *P. mirabilis* often combines with other bacteria to cause infection in patients with long-term catheterization and leads to recurrent catheter or stent blockages.<sup>49</sup> Compared with the control group including bare glass and the  $\epsilon$ -PL adsorption layer on the glass surface, the bactericidal performance of the PTB@ $\epsilon$ -PL coating against *S. aureus*, *E. coli*, and *P. mirabilis* was up to 95.42%, 99.72% and 95.29%, showing a good killing effect on common pathogenic bacteria (Fig. 2d and Fig. S14<sup>†</sup>).

We then demonstrated that the good antifouling capability of the PTB coating<sup>35</sup> would be not largely disturbed by the introduction of  $\epsilon$ -PL. After incubating the PTB@ $\epsilon$ -PL coated substrates and bare substrates in various bacteria for 24 h, these substrates were washed with PBS to remove planktonic and loosely bound bacteria. It could be seen from the scanning electron microscopy (SEM) images that mushroom-like mature biofilms were observed on the bare substrates, which were formed by the cluster of live bacteria with intact bacterial cell membrane encapsulated by the secreted EPS (Fig. 3a). In contrast, only a few bacteria were scattered on the PTB@ $\epsilon$ -PL coating, and the corresponding coating morphology was almost the same as the original coating without contact with the bacteria (Fig. S13<sup>†</sup>). For the control group, the bacterial

cells maintained their spherical (*S. aureus*) or rod shape (*E. coli* and *P. mirabilis*), but after coming in contact with the PTB@ $\epsilon$ -PL coating, a rough surface and cell deformation of the bacteria were observed, which reflected the membrane disturbance caused by  $\epsilon$ -PL in the coating. As further reflected by colony counting results, after 24 h incubation with bacteria, the number of bacteria observed on the PTB@ $\epsilon$ -PL coated surface was reduced by an average of 2–3-log compared to the bare substrate. This result indicated that the introduction of  $\epsilon$ -PL had no obvious negative effect on the ability of the coating to resist bacterial adhesion (Fig. 3b). As shown in Fig. 3c, as the number of coating times increased, the multilayer coating still maintained an excellent anti-adhesion effect towards microbes (log reduction >2). However, we also found that with the increase of the number of coating layers, the anti-bacterial adhesion efficiency of the coating decreased slightly, which may be related to the increase of surface roughness (Fig. S15<sup>†</sup>). As an antibacterial surface, the ability to resist contamination by complex media is also very important. Many antibacterial materials may become increasingly ineffective in long-term use, and this is due to conditioning of the film formed by host humoral components and bacterial debris changing the properties of the material surface and providing anchors and

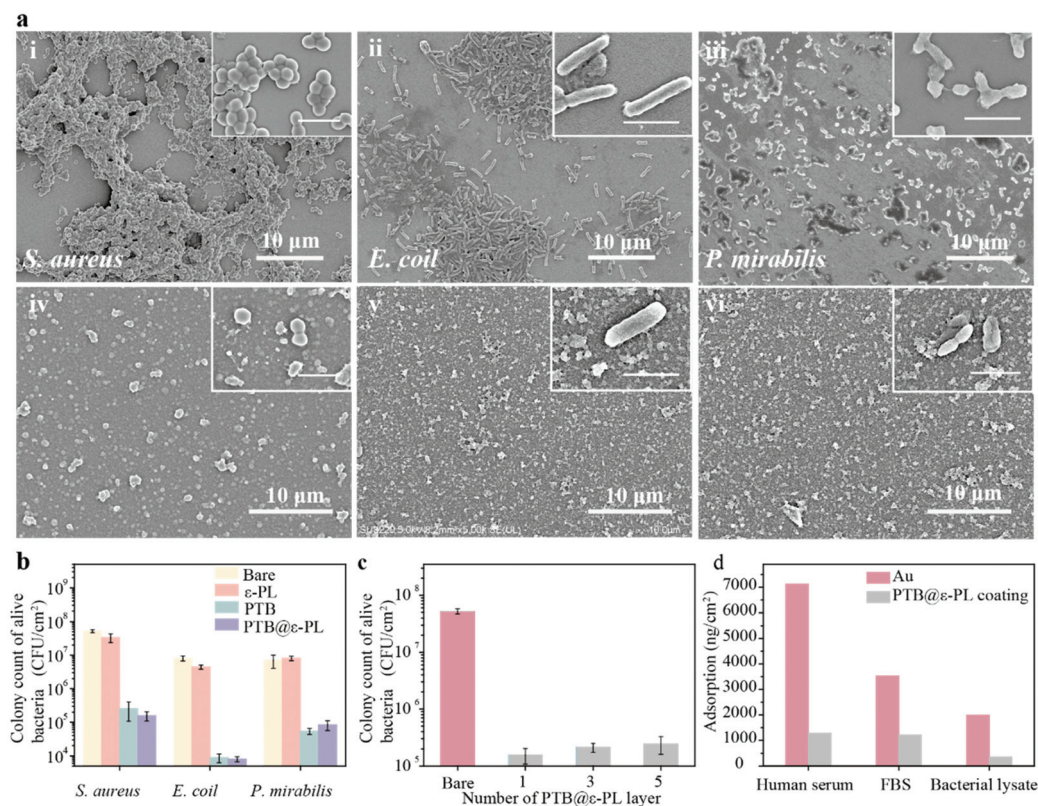


**Fig. 3** The *in vitro* anti-biofilm capacity of the PTB@ $\epsilon$ -PL coating. (a) Representative SEM images of *S. aureus* (i, iv), *E. coli* (ii, v), and *P. mirabilis* (iii, vi) adhered to bare Si (i, ii, iii) and PTB@ $\epsilon$ -PL coated Si (iv, v, vi). At high magnification, the morphology of bacteria adhering to the surface of the substrate with or without PTB@ $\epsilon$ -PL coating is shown in the inset. Scale bars are 2  $\mu$ m. (b) Number of viable bacteria recovered from bare glass,  $\epsilon$ -PL adsorption layer on glass, PTB or PTB@ $\epsilon$ -PL coated glass. (c) Effect of the coating times of the PTB@ $\epsilon$ -PL against *S. aureus* biofilm formation. The data are shown as mean  $\pm$  SD.  $n = 5$  per group. (d) Adsorption capacity of human serum, FBS and bacterial lysate on bare Au chips or Au chips coated with PTB@ $\epsilon$ -PL.

nutrients for bacterial community growth.<sup>50,51</sup> As reflected by quartz crystal microbalance with dissipation monitoring (QCM-D), the non-specific adsorption of human serum, fetal bovine serum (FBS) and bacterial lysate on PTB@ $\epsilon$ -PL coated Au chips was significantly lower than that on bare Au chips (Fig. 3d and Fig. S16<sup>†</sup>), indicating the good antifouling performance of this coating against biological fluids. Overall, the above results reflected that the PTB@ $\epsilon$ -PL coating maintained the good capacity to inhibit bacterial adhesion and biological liquid contamination while simultaneously exerting a broad-spectrum bactericidal effect.

As a coating for biomedical equipment, its stability during production and use is crucial for practical applications. To evaluate the stability of the PTB@ $\epsilon$ -PL coating, ultrasonic treat-

ment and standard 3 M adhesive tape peeling were used to simulate external mechanical forces. Autoclaving was then employed to represent the sterilization process prior to the application of medical materials, while artificial urine and saliva were used to simulate physiological conditions (Fig. 4a). After the PTB@ $\epsilon$ -PL coating experienced a series of harsh treatments typically including ultrasonication for 10 min, 3 M adhesive tape peeling, autoclaving at 121 °C for 21 min and incubation in organic solvents (*e.g.*, DMSO), artificial urine or saliva for 6 h, the coating thickness and WCA on the coating remained unchanged (Fig. 4b, c and Fig. S17<sup>†</sup>). The antimicrobial activity of the coating was also tested after the above treatments. As shown in Fig. 4d and e, the efficiency to kill bacteria and inhibit biofilm formation was consistent with

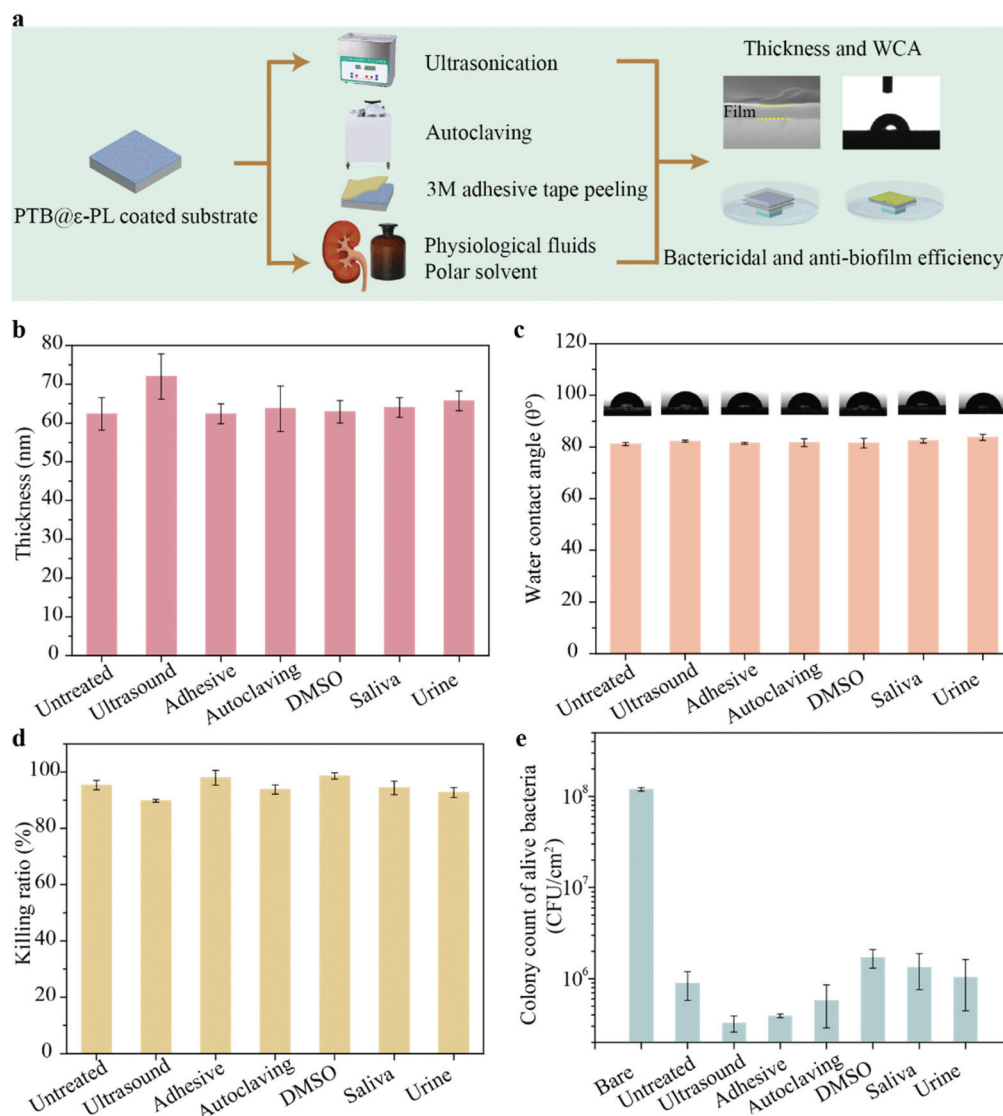


**Fig. 4** Stability evaluation of the PTB@ $\epsilon$ -PL coating under physiological and harsh conditions. (a) Cartoon diagram showing the stability test of the PTB@ $\epsilon$ -PL coating. (b) Thickness of the PTB@ $\epsilon$ -PL coating challenged by ultrasonication, 3 M adhesive tape peeling, autoclave sterilization, DMSO, saliva or urine. (c) Variation in the WCA on the glass coated with PTB@ $\epsilon$ -PL before and after challenged by physiological and harsh conditions. (d, e) The change of bactericidal capability (d) and the corresponding anti-biofilm ability (e) of the PTB@ $\epsilon$ -PL coating against *S. aureus* after the above treatments. The data are shown as mean  $\pm$  SD.  $n = 5$  per group.

those of the untreated coating. The good stability of the PTB@ $\epsilon$ -PL coating under physiological environments and extreme conditions is thus expected to sustain both robust antibacterial and anti-biofilm activity during practical stringent applications.

For the application against the infections caused by implanted devices, good biocompatibility is essential for clinical translation. We firstly used a mouse embryo fibroblast cell line (NIH/3T3) to test the cytotoxicity of the PTB@ $\epsilon$ -PL coating. The silicone rubber with or without PTB@ $\epsilon$ -PL coating presented similar cell viability as reflected by the optical density (OD) value at 490 nm even after 72 h incubation (Fig. S18<sup>†</sup>). Then, we obtained fresh rabbit blood from New Zealand white rabbits, whose cell membrane is relatively fragile, to test the hemolytic effect of the PTB@ $\epsilon$ -PL system. The results showed that the hemolysis ratio of this coating was less than 5%, which indicated good hemocompatibility based on the judging criterion for biomaterials in ASTM F756-0834 (Fig. S19<sup>†</sup>). The biocompatibility of the PTB@ $\epsilon$ -PL coating not only benefits from the biocompatibility of the PTB coating,<sup>35</sup> but also orig-

inates from the selective killing effect of  $\epsilon$ -PL based on the structural differences between bacterial and cell membranes.<sup>52</sup> For instance, cholesterol, which stabilizes the structure of cell membranes, is the main component of mammalian cell membranes but is not present in bacterial membranes. In addition, the selective toxicity of  $\epsilon$ -PL to bacteria is also due to the more negative charge on the surface of the bacteria than that on mammalian cells.

In view of the good bactericidal, universal adhesion stability to various substrates and resistance to bacterial biofilm formation, the *in vivo* experiment was further conducted in mice to evaluate the antibacterial ability of this coating in real bio-systems. All animal experiments were conducted in accordance with the guidance of the Biomedical Ethics Committee of the Medical Department of Xi'an Jiaotong University. Bare titanium and the PTB@ $\epsilon$ -PL coated titanium inoculate with *S. aureus* were implanted into both sides of the back of mice, respectively (Fig. 5a). Compared with the titanium covered by PTB@ $\epsilon$ -PL and non-implant groups, severe inflammatory response was observed in the bare implant group from 1 day

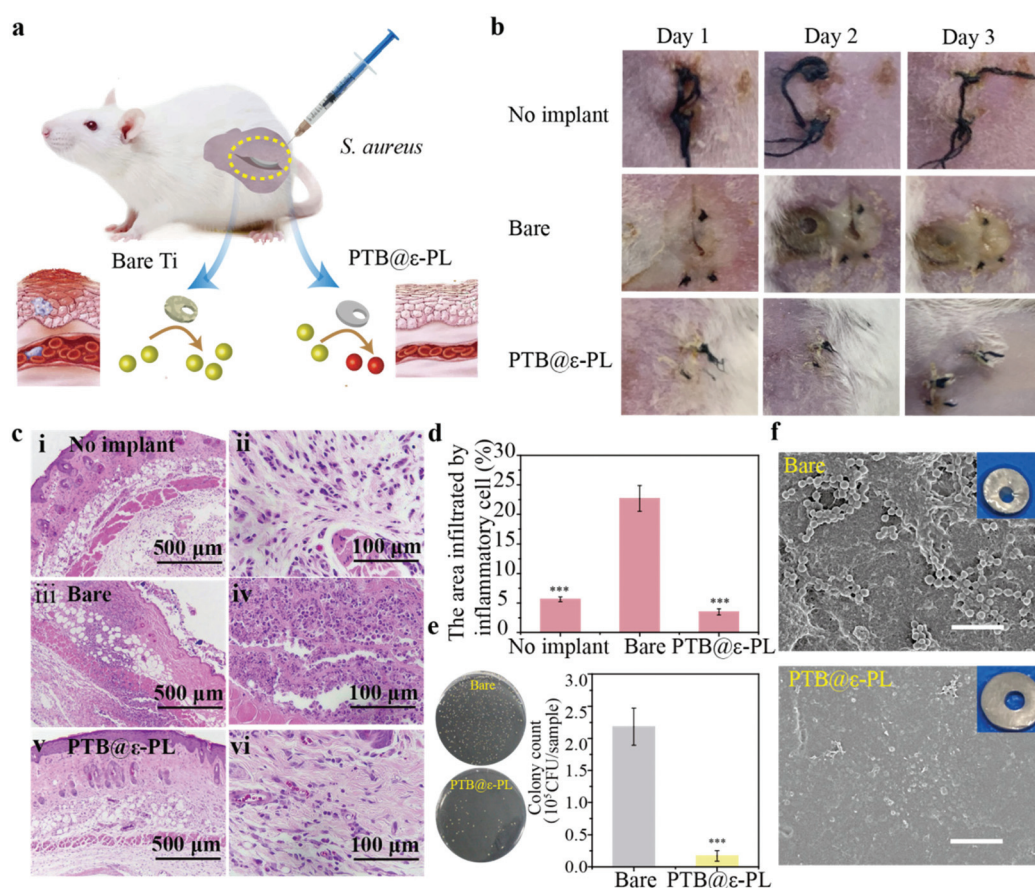


**Fig. 5** The *in vivo* antibacterial evaluation of the implants coated with the PTB@ $\epsilon$ -PL nanofilm in implant-associated bacterial infection models. (a) Schematic cartoon showing *in vivo* experiments. (b) Photographs of wounds in the control group (No implant and Bare) and the PTB@ $\epsilon$ -PL coating group for three consecutive days after the implementation of the subcutaneous infection model. (c) Tissue sections stained by H&E assay and the corresponding quantified inflammatory cell infiltration area (d). (e) Number of viable *S. aureus* recovered from the sample surface in the subcutaneous rat model ( $n = 6$ ,  $***P < 0.001$ ). (f) Optical photos (insets) and SEM images showing the surface of PTB@ $\epsilon$ -PL coated Ti and bare Ti after implantation *in vivo* for 3 days. Scale bars in (f) are 5  $\mu$ m.

after implantation, including swelling and purulent tissue around the implant, implant exposure and poor wound healing caused by skin tissue necrosis (Fig. 5b). After the animal was sacrificed, skin tissue was collected and stained with hematoxylin and eosin (H&E). Obviously, abundant infiltration of inflammatory cells was found around bare Ti accompanied by tissue necrosis. In contrast, in the tissue surrounding the implant covered with the PTB@ $\epsilon$ -PL coating, the inflammatory response was significantly attenuated, with fibroblasts and new capillaries visible and being similar to the non-implant group (Fig. 5c). A similar conclusion could also be drawn from the quantitative result of the inflammatory response, where the infiltrating area of inflammatory cells around bare Ti is 22.7%, while the value in the PTB@ $\epsilon$ -PL coating group decreased to 3.5% (Fig. 5d). By cultivating and counting bacteria on the surface of the harvested implants, it was further found that the number of bacteria on the PTB@ $\epsilon$ -PL coating was far less (92.1% decrease) than that in bare Ti (Fig. 5e), and the SEM images of the implant surface also provided consistent supporting evidence (Fig. 5f), indicating that the PTB@ $\epsilon$ -PL coating still maintained good anti-biofilm formation effect *in vivo*. Overall, the results of *in vivo* experiments demonstrated that the PTB@ $\epsilon$ -PL coating could significantly decrease the risk of bacterial colonization and infection associated with biomedical devices, and it is expected to be widely used to reduce the incidence and mortality of biomedical-associated infection complications.

### 3. Conclusion

In conclusion, a method for immobilizing  $\epsilon$ -PL on the surface through amyloid-like aggregation of BSA was developed in this study. By a simple one-step  $\epsilon$ -PL-doped amyloid-like assembly, we prepared a coating that combines the advantages of PTB (simple preparation process, universal and robust interface adhesion, excellent biocompatibility and antifouling capability) and the advantages of  $\epsilon$ -PL (wide-spectrum antibacterial activity and weak drug resistance). The results of *in vitro* antibacterial experiments show that the PTB@ $\epsilon$ -PL nanofilm is a multifunctional coating, which has the functions of broad-spectrum antibacterial effect and anti-biofilm formation against common pathogens. Due to the robust adhesion to various interfaces provided by the exposed rich functional groups in the amyloid-like aggregates, the PTB@ $\epsilon$ -PL coating can maintain good antibacterial and antifouling activity in various harsh environments (such as urine, organic solvents, autoclaving). *In vivo* experiments confirm that the PTB@ $\epsilon$ -PL coated implants can significantly reduce the infections associated with biomedical implants. Besides  $\epsilon$ -PL, this strategy also opens a window to effectively immobilize other types of bactericides such as antimicrobial peptides on versatile material surfaces. As a biocompatible biopolymer-based antibacterial coating, PTB@ $\epsilon$ -PL has broad prospects for surface modification of implants and other emerging medical indwelling equipment.

### Conflicts of interest

The authors declare that there are no conflicts of interest regarding the publication of this article.

### Acknowledgements

P. Y. is grateful for funding from the Innovation Capability Support Program of Shaanxi (no. 2020TD-024), the National Natural Science Foundation of China (no. 51673112 and 21875132), the 111 Project (no. B14041), the Fundamental Research Funds For the Central Universities (GK202007006, GK201801003, and 2017CBY004) and the Open Project of the State Key Laboratory of Supramolecular Structure and Materials (no. sklssm202030). This work was also supported by the Major Basic Research Project of Shaanxi Provincial Natural Science Basic Research Program (no. 2016ZDJC-12).

### References

- 1 K. D. Forwith, R. K. Chandra, P. T. Yun, S. K. Miller and H. D. Jampel, *Laryngoscope*, 2011, **121**, 2473–2480.
- 2 E. K. Amy, S. als. Robert, D. D. John, M. P. Glenn, L. Jamie, C. E. John and E. L. James, *J. Urol.*, 2010, **183**, 1037–1043.
- 3 Y.-K. Chao, K.-S. Liu, Y.-C. Wang, Y.-L. Huang and S.-J. Liu, *Chest*, 2013, **144**, 193–199.
- 4 S. Moon, S.-G. Yang and K. Na, *Biomaterials*, 2011, **32**, 3603–3610.
- 5 F. Arab Hassani, R. P. Mogan, G. G. L. Gammad, H. Wang, S.-C. Yen, N. V. Thakor and C. Lee, *ACS Nano*, 2018, **12**, 3487–3501.
- 6 F. A. Hassani, W. Y. X. Peh, G. G. L. Gammad, R. P. Mogan, T. K. Ng, T. L. C. Kuo, L. G. Ng, P. Luu, S.-C. Yen and C. Lee, *Adv. Sci.*, 2017, **4**, 1700143.
- 7 K. G. Neoh, M. Li, E. T. Kang, E. Chiong and P. A. Tambyah, *J. Mater. Chem. B*, 2017, **5**, 2045–2067.
- 8 C. R. Arciola, D. Campoccia and L. Montanaro, *Nat. Rev. Microbiol.*, 2018, **16**, 397–409.
- 9 V. D. Bui, J. W. Mwangi, A.-K. Meinshausen, A. J. Mueller, J. Bertrand and A. Schubert, *Surf. Coat. Technol.*, 2020, **383**, 125254.
- 10 A. Besinis, S. D. Hadi, H. R. Le, C. Tredwin and R. D. Handy, *Nanotoxicology*, 2017, **11**, 327–338.
- 11 R. Wang, K. G. Neoh, E. T. Kang, P. A. Tambyah and E. Chiong, *J. Biomed. Mater. Res., Part B*, 2015, **103**, 519–528.
- 12 R. Bayston and R. D. G. Milner, *J. Clin. Pathol.*, 1981, **34**, 1057–1062.
- 13 M. Cloutier, D. Mantovani and F. Rosei, *Trends Biotechnol.*, 2015, **33**, 637–652.
- 14 H. Yu, X. Chen, J. Cai, D. Ye, Y. Wu and P. Liu, *J. Biomater. Sci., Polym. Ed.*, 2019, **30**, 64–76.
- 15 Q. Yu, Z. Wu and H. Chen, *Acta Biomater.*, 2015, **16**, 1–13.

- 16 J. M. L. Iyamba, D. T. Okombe, F. N. Zakanda, T. K. Malongo, J. W. Unya, C. M. Lukukula and N. za B. Takaisi Kikuni, *Pan Afr. Med. J.*, 2016, **25**, 1–8.
- 17 A. M. Carmona-Ribeiro and L. D. de Melo Carrasco, *Int. J. Mol. Sci.*, 2013, **14**, 9906–9946.
- 18 D. He, Y. Yu, F. Liu, Y. Yao, P. Li, J. Chen, N. Ning and S. Zhang, *Chem. Eng. J.*, 2020, 382.
- 19 R. Chen, M. D. P. Willcox, K. K. K. Ho, D. Smyth and N. Kumar, *Biomaterials*, 2016, **85**, 142–151.
- 20 X. Li, P. Li, R. Saravanan, A. Basu, B. Mishra, S. H. Lim, X. Su, P. A. Tambyah and S. S. J. Leong, *Acta Biomater.*, 2014, **10**, 258–266.
- 21 M. D. P. Willcox, E. B. H. Hume, Y. Aliwarga, N. Kumar and N. Cole, *J. Appl. Microbiol.*, 2008, **105**, 1817–1825.
- 22 Y. Dang, M. Quan, C. M. Xing, Y. B. Wang and Y. K. Gong, *J. Mater. Chem. B*, 2015, **3**, 2350–2361.
- 23 C. M. Xing, F. N. Meng, M. Quan, K. Ding, Y. Dang and Y. K. Gong, *Acta Biomater.*, 2017, **59**, 129–138.
- 24 S. Yan, H. Shi, L. Song, X. Wang, L. Liu, S. Luan, Y. Yang and J. Yin, *ACS Appl. Mater. Interfaces*, 2016, **8**, 24471–24481.
- 25 Y. Zhang, X. Zhang, Y. Q. Zhao, X. Y. Zhang, X. Ding, X. Ding, B. Yu, S. Duan and F. J. Xu, *Biomater. Sci.*, 2020, **8**, 997–1006.
- 26 P. C. Nalam, H.-S. Lee, N. Bhatt, R. W. Carpick, D. M. Eckmann and R. J. Composto, *ACS Appl. Mater. Interfaces*, 2017, **9**, 12936–12948.
- 27 B. Wang, H. Liu, Z. Wang, S. Shi, K. Nan, Q. Xu, Z. Ye and H. Chen, *J. Mater. Chem. B*, 2017, **5**, 1498–1506.
- 28 P. Yuan, X. Qiu, X. Wang, R. Tian, L. Wang, Y. Bai, S. Liu and X. Chen, *Adv. Healthcare Mater.*, 2019, **8**, 1–9.
- 29 Q. Wang, L. Wang, L. Gao, L. Yu, W. Feng, N. Liu, M. Xu, X. Li, P. Li and W. Huang, *J. Mater. Chem. B*, 2019, **7**, 3865–3875.
- 30 C. Zhou, Y. Wu, K. R. V. Thappeta, J. T. L. Subramanian, D. Pranantyo, E. T. Kang, H. Duan, K. Kline and M. B. Chan-Park, *ACS Appl. Mater. Interfaces*, 2017, **9**, 36269–36280.
- 31 C. Yang, X. Ding, R. J. Ono, H. Lee, L. Y. Hsu, Y. W. Tong, J. Hedrick and Y. Y. Yang, *Adv. Mater.*, 2014, **26**, 7346–7351.
- 32 X. Xiong, Z. Wu, Q. Yu, L. Xue, J. Du and H. Chen, *Langmuir*, 2015, **31**, 12054–12060.
- 33 K. Lim, R. Rong, Y. Chua, H. Bow, P. Anantharajah, K. Hadinoto, S. Su and J. Leong, *Acta Biomater.*, 2015, **15**, 127–138.
- 34 C. Li, L. Xu, Y. Y. Zuo and P. Yang, *Biomater. Sci.*, 2018, **6**, 836–841.
- 35 X. Hu, J. Tian, C. Li, H. Su, R. Qin, Y. Wang and X. Cao, *Adv. Mater.*, 2020, **2000128**, 1–11.
- 36 H. Liu, H. Pei, Z. Han, G. Feng and D. Li, *Food Control*, 2015, **47**, 444–450.
- 37 Z. Tan, Y. Shi, B. Xing, Y. Hou, J. Cui and S. Jia, *Bioresour. Bioprocess.*, 2019, **6**, 11.
- 38 Y. Zhao, F. Li, M. T. Carvajal and M. T. Harris, *J. Colloid Interface Sci.*, 2009, **332**, 345–353.
- 39 J. Liu, Y. Y. Shim, Y. Wang and M. J. T. Reaney, *Food Hydrocolloids*, 2015, **49**, 95–103.
- 40 J. N. Liu, S. L. Chang, P. W. Xu, M. H. Tan, B. Zhao, X. D. Wang and Q. S. Zhao, *J. Agric. Food Chem.*, 2020, **68**, 1101–1109.
- 41 Y. Xu, Y. Liu, X. Hu, R. Qin, H. Su, J. Li and P. Yang, *Angew. Chem., Int. Ed.*, 2020, **59**, 2850–2859.
- 42 W. Ji, C. Yuan, P. Chakraborty, S. Gilead, X. Yan and E. Gazit, *Commun. Chem.*, 2019, **2**, 65.
- 43 R. Qin, Y. Liu, F. Tao, C. Li, W. Cao and P. Yang, *Adv. Mater.*, 2019, **31**, 1–11.
- 44 S. S. S. Wang, K. N. Liu and B. W. Wang, *Eur. Biophys. J.*, 2010, **39**, 1229–1242.
- 45 J. Gu, Y. Su, P. Liu, P. Li and P. Yang, *ACS Appl. Mater. Interfaces*, 2017, **9**, 198–210.
- 46 R. E. Holmlin, X. Chen, R. G. Chapman, S. Takayama and G. M. Whitesides, *Langmuir*, 2001, **17**, 2841–2850.
- 47 F. Yang, F. Tao, C. Li, L. Gao and P. Yang, *Nat. Commun.*, 2018, **9**, 5443.
- 48 M. Lorenzetti, I. Dogša, T. Stošicki, D. Stopar, M. Kalin, S. Kobe and S. Novak, *ACS Appl. Mater. Interfaces*, 2015, **7**, 1644–1651.
- 49 M. Ramstedt, I. A. C. Ribeiro, H. Bujdakova, F. J. M. Mergulhão, L. Jordao, P. Thomsen, M. Alm, M. Burmølle, T. Vladkova, F. Can, M. Reches, M. Riool, A. Barros, R. L. Reis, E. Meaurio, J. Kikhney, A. Moter, S. A. J. Zaat and J. Sjollem, *Macromol. Biosci.*, 2019, **1800384**, 1–26.
- 50 T. R. Garrett, M. Bhakoo and Z. Zhang, *Prog. Nat. Sci.*, 2008, **18**, 1049–1056.
- 51 M. T. Buhmann, P. Stiefel, K. Maniura-Weber and Q. Ren, *Trends Biotechnol.*, 2016, **34**, 945–948.
- 52 J. Hiraki, T. Ichikawa, S. I. Ninomiya, H. Seki, K. Uohama, H. Seki, S. Kimura, Y. Yanagimoto and J. W. Barnett, *Regul. Toxicol. Pharmacol.*, 2003, **37**, 328–340.